APH N.S., Heavy Ion Physics 17/1 (2003) 000–000

HEAVY ION PHYSICS
©**Akadémiai Kiadó**

The Critical Exponent of Nuclear Fragmentation

A. Barrañón,[1] R. Cárdenas,[2] C.O. Dorso[3] and J.A. López[2]

[1] Universidad Autónoma Metropolitana – Azcapotzalco, México, D.F., México
[2] University of Texas at El Paso, El Paso, Texas 79968, USA
[3] Universidad de Buenos Aires, Nuñez 1428, Buenos Aires, Argentina

Received 15 July 2002

Abstract. Nuclei colliding at energies in the MeV's break into fragments in a process that resembles a liquid-to-gas phase transition of the excited nuclear matter. If this is the case, phase changes occurring near the critical point should yield a "droplet" mass distribution of the form $\approx A^{-\tau}$, with τ (a critical exponent universal to many processes) within $2 \leq \tau \leq 3$. This critical phenomenon, however, can be obscured by the finiteness in space of the nuclei and in time of the reaction. With this in mind, this work studies the possibility of having critical phenomena in small "static" systems (using percolation of cubic and spherical grids), and on small "dynamic" systems (using molecular dynamics simulations of nuclear collisions in two and three dimensions). This is done investigating the mass distributions produced by these models and extracting values of critical exponents. The specific conclusion is that the obtained values of τ are within the range expected for critical phenomena, i.e. around 2.3, and the grander conclusion is that phase changes and critical phenomena appear to be possible in small and fast breaking systems, such as in collisions between heavy ions.

Keywords: critical phenomena, heavy-ion reactions, percolation, multifragmentation
PACS: 25.70.Pq

1. Introduction

Experimental studies of phase transformations in nuclear matter began in the mid 80's when it became possible to achieve collisions between heavy nuclei with energies in the tens of MeV's per nucleon [1–8]. Now that it is generally accepted that nuclei can undergo transformations between liquid and gaseous phases, modern research focuses on the exciting possibility of finding critical phenomena, i.e. changes near the critical point, in nuclear reactions [9–11].

1219-7580/03/ $ 25.00

Just like gases present no correlations between neighboring particles, and liquids exhibit a strong two-body correlation produced by nearest neighbors, near the critical point the correlations grow to include all particles in the system. The near-critical point behavior is characterized by a loss of distance and time scales, which in turns makes all critical phenomena have similar characteristics, independent of the specific details of the system. Such a loss of scale results, for instance, in a characteristic mass distribution of the droplets produced during the phase change. Fisher's droplet model predicts a mass yield of the form of a power law $Y \propto A^{-\tau}$, with the exponent τ, one of the universal "critical exponents", within $2 \leq \tau \leq 3$.

Although recent experimental studies indicate that critical phenomena is feasible in nuclear systems [12], it has not been definitely proven that finite and transient systems can support such phenomena. Since in small and rapid processes the largest scales are set by the size of the system and the duration of the reaction, scaleless critical phenomena are not guaranteed to exist. Thus the motivation of the present study: to test the feasibility of such phenomena in *fast* and *small* dynamical systems, such as nuclear reactions.

To determine the existence of nuclear critical phenomena, signatures of criticality are sought in this work with models commonly used to study nuclear reactions. To study the effect of finite sizes and times, models based on percolation model and molecular dynamics have been adapted to represent small "static" systems and small "dynamical" systems. Specifically, the models will be used to produce phase transition-like data, such as "droplet" mass distributions, which then will be dissected to extract, as best as possible, those data produced near the critical point. The resulting subsets will then be used to extract critical exponents. A determination of a power-law looking yield with a τ close to the expected values would be an indication of the feasibility of criticality in small and transient processes, such as in heavy-ion reactions.

The manuscript, in Section 2, introduces the basic ingredients of nuclear thermodynamics and critical phenomena. Section 3 presents a search of a critical breakup using the percolation model. This is also investigated with molecular dynamics simulations of collisions in Section 4. Finally, conclusions are presented in Section 5.

2. Nuclear Thermodynamics and the Critical Exponent τ

To justify the expectation of finding critical phenomenon in nuclear reactions, this section introduces the minimum ingredients needed to obtain a sketch of the nuclear equation of state (EOS) and its phase diagram.

Any model representing a cold ($T = 0$) nucleus at normal density (n_0) should yield an energy per nucleon of $\varepsilon = -8$ MeV with vanishing pressure (since a nucleus is stable at this density), and with compressibility on the order 100 MeV $< K <$ 300 MeV, as observed in experiments of nuclear oscillations [13]. One such model [14, 7] that represents the nucleus as a collection of neutrons and protons in a

potential well interacting through a phenomenological interaction, yields a phase diagram like that of Fig. 1.

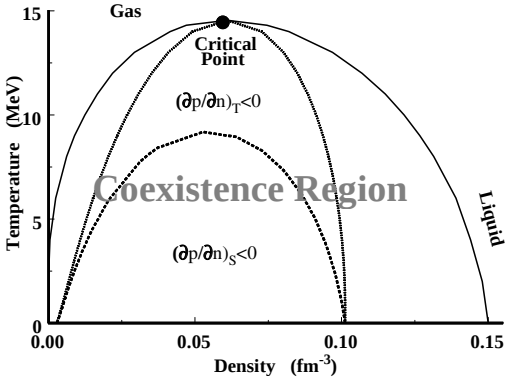

Fig. 1. Phase diagram of nuclear matter. For the EOS used, the critical point is at $n_c = 0.061$ fm^{-3} and $T_c = 14.542$ MeV. Nuclear matter goes from a uniform phase to a mixed phase if it enters the coexistence region.

Inside the spinodal regions, where $(\partial p/\partial n)_T < 0$, or $(\partial p/\partial n)_S < 0$, the system is unstable as it responds to an increase of the density n with a reduction of the pressure p and a further increase of the density. Another region of interest where, although $\partial p/\partial n > 0$, no extra energy is needed to remove or bind a nucleon from a nucleus, is the *coexistence* region, where uniform nuclear matter breaks into phases just like a van der Waals type liquid. Liquid-to-gas changes occur whenever the system attains densities and temperatures inside these regions. If these features of the phase diagram for infinite system exist for finite systems, it might be feasible that heavy-ion collisions could drive nuclei into the coexistence region where a transformation of a liquid system into a liquid–gas mixture could take place through nucleation.

According to fluctuation theory [15], the probability of having a liquid drop of radius r and A nucleons in a vapor at temperature T is given by $P_r(A) \propto e^{-\Delta G/T}$, with ΔG being the difference in Gibbs free energy between phases. For spherical drops, using the ΔG given by the bulk, surface and curvature terms, it yields [14]:

$$P_r(A) = Y_0 A^{-\tau} e^{-\left[(\mu_l - \mu_g)A + 4\pi r_0^2 \sigma(T) A^{2/3}\right]/T} \ ,$$

with Y_0 a normalization constant. This general functional form, which displays a U-shaped behavior, applies in the supersaturated region. In the coexistence region, however, $(\mu_l - \mu_g) = 0$, and $P_r(A) = Y_0 A^{-\tau} \exp[-4\pi r_0^2 \sigma(T) A^{2/3}/T]$, describing a power law decay times an exponential fall-off that dominates for large masses.

Finally, at the critical point $(\mu_l - \mu_g) = 0$ but since the liquid and vapor are indistinguishable at this point, the surface tension vanishes, $\sigma(T_c) = 0$, and the yield distribution is simply

$$P_r(A) = Y_0 A^{-\tau} \ , \tag{1}$$

which is a pure power law and, as such, free of scales. The exponent τ appearing in the distribution (1) of the size of the droplets, is known as a critical exponent as it is a unitless constant with a value common to many diverse systems. For our case τ can be obtained from a power-law fit to mass distributions, as shown next.

Fisher's droplet model (FDM) of nucleation [16] refines the probability (1) to yield a critical average droplet mass distribution normalized to the size of the system of the form

$$n_A = q_0 A^{-\tau} \tag{2}$$

with a proportionality constant q_0 that can be obtained from the first moment, $M_1 = \sum_A n_A A$, of the normalized (i.e. $M_1 = 1$) mass distribution. Since at the critical point $q_0 = n_A A^\tau$, the moment becomes $M_1 = q_0 \sum_A A^{(1-\tau)} = 1$, and q_0 can then be obtained via the Riemann-ζ function: $q_0 = 1/\sum_A A^{(1-\tau)}$. Notice that, since at the critical point any excess bulk liquid drop must be excluded, the sum runs only over clusters in the gaseous phase, effectively treating the yield as part of an infinite system.

In summary, to obtain τ, expression (2) should be used as a single parameter fit of the cluster mass distribution, normalized to the size of the system, and with $q_0 = 1/\sum_A A^{(1-\tau)}$. If τ is to be extracted from contaminated data, i.e. containing critical and non-critical data, only the part of the mass spectra that best reproduces a power law should be used [17]. This technique is used next with cluster data generated by percolation, and in Section 4 with molecular dynamics.

3. The Critical Exponent τ from Percolation

Before obtaining a τ from percolation, the question of whether a τ-producing critical phenomenon can exist in percolation is first addressed. Arguments are presented that indicate that such a power-law mass distribution can exist in general lattices. These arguments, however, only apply to infinite systems, and the question for finite systems must be answered by direct computations.

Percolation was introduced to the study of nuclear fragmentation by Bauer [18, 19], for the details of this calculational procedure, see Ref. [20]. A percolating cluster is one in which activated bonds extend from one side of the lattice to the opposite one. For infinite systems there is a sharp "critical site occupation probability" p_c, above which the probability of finding a percolation cluster is 1, whereas below p_c it is 0. For finite lattices the transition from one regime to the other is smooth, i.e. the probability of finding a percolating cluster is different from 0 for any probability.

If the sites in a one-dimensional lattice become occupied or empty according to a random probability p, some clusters of neighboring occupied sites of different sizes

will appear. The number of clusters of length s, will be given by $n_s(p) = p^s(1-p)^2$, and a percolating cluster will only happen when all the sites of the chain occupied. Thus the percolation threshold is unity, $p_c = 1$, and there are no percolating clusters for p below unity. It is possible to extend these results to the case of a general lattice. Without entering into details [20], it can be shown that in any percolating lattice, the average number of clusters of size s satisfies $n_s \propto p^s(1-p)^{2+(z-2)s}$. And if at $p = p_c$, n_s decays exponentially and a power law of the form $n_s(p_c) \propto s^{-\tau}$ is plausible for large s.

Since near the critical point the typical cluster size, s becomes very large, Stauffer proposed a generalization of the FDM for $p \sim p_c$

$$n_s(p) \sim s^{-\tau} f(z)\,, \tag{3}$$

where the scaling variable is $z = (p-p_c)s^{\sigma}$, σ is another critical exponent, and $f(z)$ is the scaling function with only one maximum located below the critical point, $f(0) = 1$.

In conclusion, excepting a small difference in the scaling function $f(z)$, any general percolation model offers a power-law distribution of clusters of the form similar to Fisher's model. Thus one can use the percolation model to explore, for instance, the effect of the size and geometry of the grid on a possible phase transition.

3.1. The critical exponent τ from the percolation of a cubic grid

Consider a square cubic lattice with some of the sites connected or not according to a random probability p or $(1-p)$. Then check to see if a percolating cluster has been formed with the assigned p. After repeating for different values of p, the smallest value at which a percolating cluster is formed is taken as the percolation probability p_c. The change from having disconnected clusters to having a percolating cluster is a phase transition. We take advantage of this and obtain values of the critical exponent τ from the distribution of cluster sizes produced by this method.

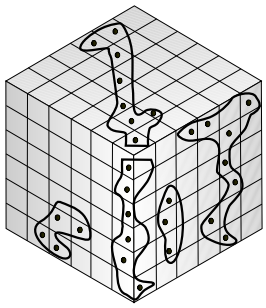

Fig. 2. Graphical representation of the percolation of a cubic lattice

Bond-building computations were performed in three-dimensional simple cubic lattices of $6 \times 6 \times 6$ (i.e. 216) sites using a lattice probability p_l as the control parameter. All values of the bond probability, P_{b_i}, were randomly chosen from a uniform distribution in $(0, 1)$ for the ith bond. If P_{b_i} was less than p_l then the ith bond was activated joining two sites into a cluster. This process was performed for each bond in the lattice. For low values of p_l, few bonds were formed resulting in a high multiplicity of small clusters; a distribution analogous to the gaseous phase of a fluid. At high values of p_l, many bonds were formed resulting in a multiplicity of mostly large clusters, analogous to a liquid phase of a fluid.

100 000 lattice realizations were generated using 100 values of p_l varying from 0 to 1, and the cluster multiplicity, m, the number clusters of size A per lattice site, was obtained for each p_l. The multiplicity with the best power-law like distribution was used to determine τ. Following the FDM, the biggest fragment was removed for the "liquid-branch", i.e. below the critical multiplicity, m_c. Since, in this case, we do not know m_c a priori, all clusters with $A \geq 53$ were excluded. Likewise, clusters of size $A = 1$ were also excluded. The extracted parameters, τ, q_0 and p_c do not depend on the fit range.

The calculations were performed for $0.02\ A_{\rm tot} < A_{\rm tot} = 144 < 0.15\ A_{\rm tot}$ to avoid finite sizes effects. The goodness of the fits of the power-law were determined by the χ^2 method looking at the minimum square of $\log(Y(A)) - \log(q_0) + \tau \log(A)$ for each probability P_l. The cluster distribution that is best described by the power law should show a minimum in χ^2 indicating proximity to the critical point. Away from the critical point the power law is modified by a scaling function of the form $f(z) = A \exp(g)$, with g constant, and thus, fits to a single parameter power law should become worse.

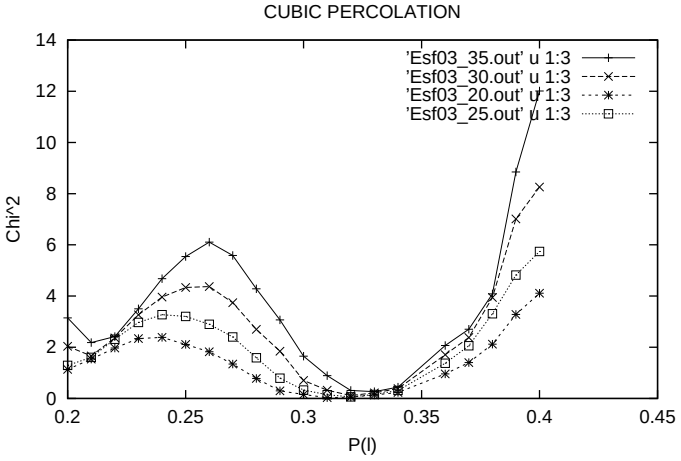

Fig. 3. Goodness of power-law fit, χ^2, as a function of P_l

Figure 3 shows the behavior of the χ^2 obtained as a function of the control parameter P_l. A minimum in χ^2 is observed for fits in the mid P_l range indicating the location of a cluster distribution which is best fitted by a single parameter power law. The best fit of the mass spectra gives a value of $\tau = 2.32 \pm 0.02$ at $m_c = 22 \pm 1$ $q_0 = 0.18 \pm 0.01$ and a $\chi^2 = 2.70$. An uncertainty of one unit of multiplicity is assigned to m_c to take in account the relatively low values of χ^2 of the neighboring fits. The lower χ^2 value is due the finer bins over which the cluster distribution were grouped. Figure 4 shows the best power law for $p_l = 0.32$.

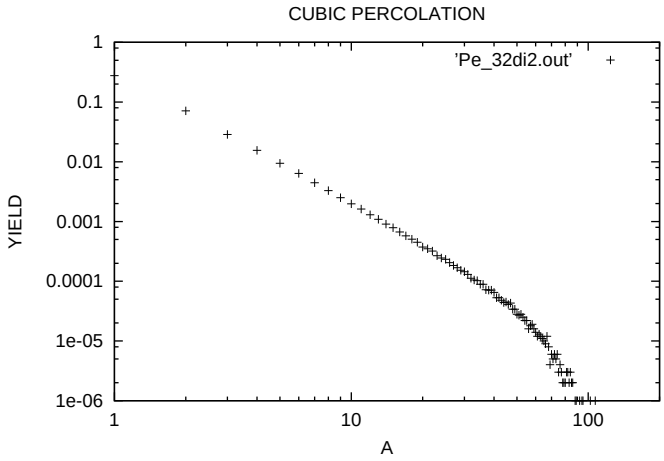

Fig. 4. Mass distribution obtained from the percolation of a cubic grid that was best fitted by a power law. The corresponding p_l was 0.32.

The observed agreement between the values of the exponents determined by this procedure and the canonical values in various universality classes, is then significant because these have been determined solely by the behavior of the cluster distribution so analyzed.

3.2. The critical exponent τ from the percolation of a spherical grid

To explore the effect of the shape of the grid on the value of τ, a spherical lattice, as that represented in Fig. 5, was analyzed in the same fashion and with the same equations for q_0 and n_A as done for the cubic grid before. Even though the outer shape of the grid is spherical, internally it has the same cubic structure as before. The "spherical" lattice was constructed out a simple cubic lattice of $6 \times 6 \times 6$, but now with the edges cut. This produced an approximately spherical grid of 203 sites.

Again, 100 000 of these grids were percolated with varying lattice probabilities p_l as described before. The resulting cluster size distribution was fitted by a power law using p_l as a control parameter. Figure 6 shows the goodness of power-law fits obtained, χ^2, as a function of P_l. The values obtained for τ the critical exponent

and p_l are $\tau = 2.32$, for $p_l = 0.32$, in total agreement with the results of the cubic grid. Figure 7 shows the best power law fit obtained for $p_l = 0.32$.

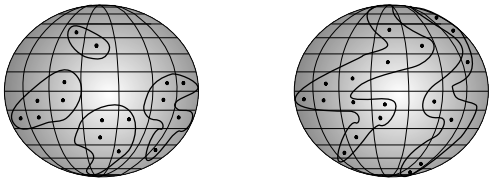

Fig. 5. Graphical representation of the percolation of a spherical lattice

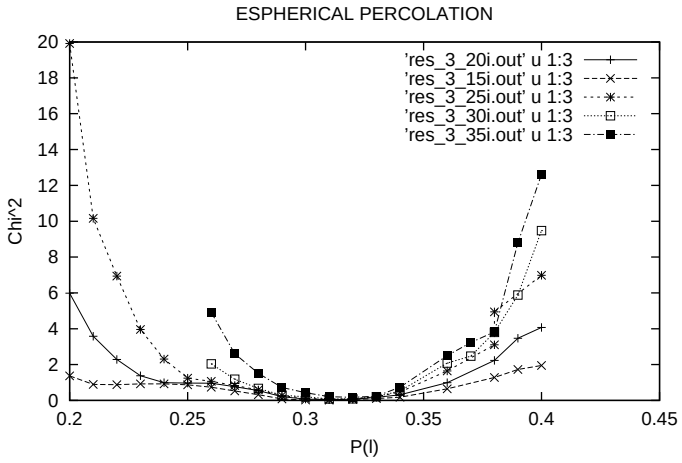

Fig. 6. Goodness of power-law fit, χ^2, as a function of P_l

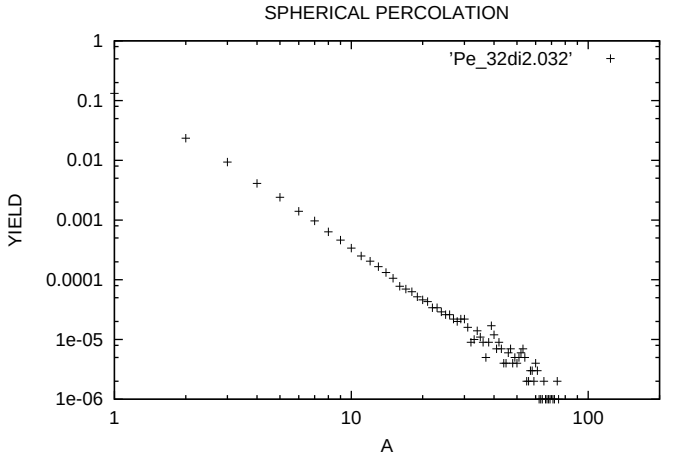

Fig. 7. Mass distribution (obtained from the percolation of a spherical grid) that was best fitted by a power law. The corresponding p_l was 0.32.

4. The Critical Exponent τ from Simulated Collisions

At a difference with percolation where critical phenomena is known to exist, nuclear fragmentation, being produced by small nuclei in brief reactions, is not guaranteed to exhibit criticality. Here this question is addressed with molecular dynamics (MD). After introducing the model and the techniques for detecting fragments, MD will be used to study the fragmentation produced by collisions Lennard–Jones drops and of Pandharipande "nuclei". The resulting clusters will be analyzed to obtain signatures of critical phenomena, namely values of τ.

4.1. Molecular dynamics

Heavy-ion collisions have been studied with the method of "Molecular Dynamics", which, although based on Newtonian mechanics, it is the only one that can describe changes of phase, hydrodynamic flow, and non-equilibrium dynamics without adjustable parameters. The virtues of molecular dynamics for the study of nuclear collisions have been stated in the current literature [21].

In this chapter, the evolution of the collision of two "nuclei" will be modeled with MD. The nucleons will be treated as point particles subjected to potential forces (Lennard–Jones potential in Section 4.3 and Pandharipande potential in 4.4). The colliding nuclei are constructed as self-bound clusters of particles with some specific geometry (two-dimensional circles in Section 4.3 and spheres in 4.4). The collision is simulated by boosting one of these nuclei onto the other one, and integrating the coupled equations of motion numerically using a velocity-Verlet algorithm. The accuracy of the integration is assessed by enforcing energy conservation to a high degree.

Following the dynamics of thousands of these collisions at different energies, enough information can be gathered to understand the fragmentation of the "nuclei", and, hopefully, to obtain a critical exponent τ from the mass distribution of the produced fragments. To reach this stage, however, the information provided by MD, which is given in terms of point particles, should be first transformed into fragments.

4.2. Fragment recognition

To transform the particle information provided by MD into fragment information, a fragment-recognition algorithm is needed. The simplest cluster definition is the "Minimum Spanning Tree" (MST) and it is based on correlations in configuration space: a particle i belongs to a cluster C if there is another particle j that belongs to C and $|\mathbf{r_i} - \mathbf{r_j}| \leq r_{cl}$, where r_{cl} is a parameter called the clusterization radius. The main drawback of MST is that, since only correlations in $\mathbf{r}$-space are used, it neglects completely the effect of momentum giving incorrect information for dense systems.

A more robust algorithm is based on the "Most Bound Partition" of the system [22], i.e. on the set of clusters $\{C_i\}$ for which the sum of the fragment internal energies attains its minimum value:

$$\begin{aligned} \{C_i\} &= \underset{\{C_i\}}{\operatorname{argmin}} \left[E_{\{C_i\}} = \textstyle\sum_i E_{\rm int}^{C_i}\right], \\ E_{\rm int}^{C_i} &= \sum_i \Big[\sum_{j\in C_i} K_j^{cm} + \sum_{\substack{j,k\in C_i \\ j\le k}} V_{j,k}\Big], \end{aligned} \tag{4}$$

where the first sum is over the clusters of the partition, K_j^{cm} is the kinetic energy of particle j measured in the center of mass frame of the cluster which contains particle j, and V_{ij} stands for the inter-particle potential. The algorithm that finds the most-bound partition is known as the "Early Cluster Recognition Algorithm" (ECRA), which has been used extensively in many fragmentation studies [21–23] and has helped to discover that excited drops break very early in the evolution.

4.3. The critical exponent τ from collisions of Lennard–Jones drops

Here we study the behavior of a two-dimensional system composed by classical particles that interact via a two-body Lennard–Jones potential:

$$V(r) = 4\epsilon\left[\left(\frac{\sigma}{r}\right)^{12} - \left(\frac{\sigma}{r_{\rm cut}}\right)^{12} - \left(\frac{\sigma}{r}\right)^{6} + \left(\frac{\sigma}{r_{\rm cut}}\right)^{6}\right], \tag{5}$$

where $r_{\rm cut}$ is the cut off radius, the potential is taken as zero for $r \ge r_{\rm cut}$. We consider $r_{\rm cut} = 3\sigma$. The unit of time and energy are $t_0 = \sqrt{\sigma^2 m/48\epsilon}$ and ϵ, respectively. Head-on projectile–target collisions are studied using a target and a projectile consisting of a randomly-oriented two-dimensional drop of 74-particles (i.e. *Germanium* or *Arsenic*) on its "ground state", $\epsilon_0 \sim -2.8\epsilon$. The velocity-Verlet algorithm is applied with a time step of $t_{\rm int} = 0.0025 t_0$ and an energy conservation better than 0.05%.

The kinetic projectile energies go from $E_{\rm beam} = 18\epsilon$ to 2520ϵ in the center of mass reference frame with two hundred collisions performed for each energy. In this energy range several types of dynamical evolutions are found: from projectile adsorption by the droplet surface, up to events with a mass spectrum with an exponential decay.

As explained elsewhere [17], in the collision prompt nucleons are knocked out by collisions between projectile and target nucleons. Initially, an excited compound nucleus with fewer than 148 nucleons is formed, which may expand and cool down to the neighborhood of the critical point where clusters might condense from a high temperature low density vapor of nucleons. The charge and mass of the compound nucleus, Z_0 and A_0, were determined for each event by subtracting the prompt particles from the total nucleus. The resulting cluster distribution was then normalized to the size of the system, $n_{A_f} = N_{A_f}/A_0(m)$ and fitted to power law (2).

A problem arises in the (?)obtention(?) of τ when data coming from breakups near the critical point is mixed with that produced at other points in the phase diagram. The extraction of critical data from this mix is not an easy task but it can be accomplished with the methodology of [17]. Simply stated, the full set of data is partitioned in smaller sets corresponding to different values of the multiplicity, and each set is then fitted to the power law using a single parameter fit. The goodness of these fits is estimated simply by a χ^2, and the τ of the best set is taken as the critical exponent.

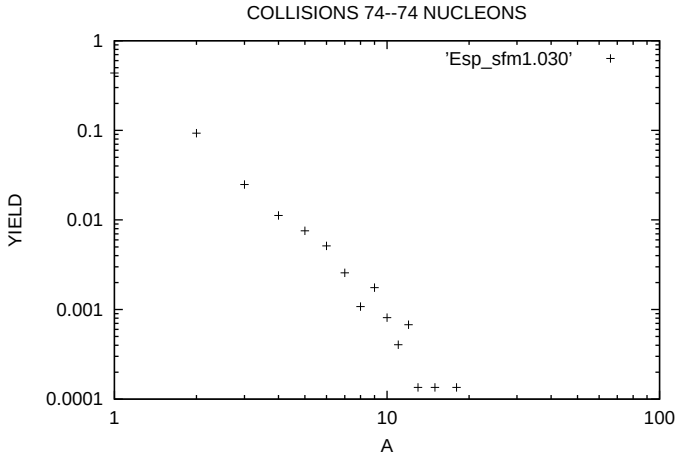

Fig. 8. Yield produced by MD simulations of 2-D collisions

To avoid finite sizes effects, this fitting procedure was performed in the mass range between $0.03A_{\rm tot}$ and $0.15A_{\rm tot}$, with $A_{\rm tot} = 140$. The obtained critical exponent was found to be $\tau \cong 2.32 \pm 0.02$ in perfect agreement to the percolation results. Figure 8 shows the mass yield with the best power law fit.

4.4. The critical exponent τ from collisions of "realistic" nuclei

A more realistic MD model, nicknamed the "Latino model" [24] to reflect its Latin American origin, was also used. This three dimensional model uses two-body potentials that reproduce the empirical energy and density of nuclear matter, as well as realistic effective scattering cross sections.

The Pandhariphande potentials differentiate between different types of nucleons: $V_{np(r)}$(neutron–proton) is attractive at large r and repulsive at small r, $V_{nn}(r)$ (neutron–neutron) and $V_{pp}(r)$ (proton–proton) are purely repulsive interactions. Additionally the Coulomb term is also included. The "nuclear" part of the interaction potential is [25]:

$$\begin{aligned} V_{np}(r) &= V_r \left[\exp(-\mu_r r)/r - \exp(-\mu_r r_c)/r_c\right] \\ &\quad - V_a \left[\exp(-\mu_a r)/r - \exp(-\mu_a r_a)/r_a\right] , \end{aligned}$$

$$V_{nn}(r) \quad = \quad V_{pp}(r) = V_0 \left[\exp(-\mu_0 r)/r - \exp(-\mu_0 r_c)/r_c\right] , \tag{6}$$

where $r_c = 5.4$ fm is a cutoff radius. For simplicity in numerical calculations, $V_{nn}(r > r_c) = V_{np}(r > r_c) = 0$. In this way, no bound state of identical nucleons can exist. The ground state of this classical nuclear matter interacting is a simple cubic solid. The values of the parameters of the Yukawa potentials are given in [25] and give a corresponding equation of state with a compressibility of about 250 MeV.

The nuclei used here are liquid-like spherical drops with the right number of protons and neutrons, and placed on the "ground" state using molecular dynamics. After the spherical system nuclear system is produced at a rather high temperature confined in a steep spherical potential, it is allowed to cool until it reaches a self-contained state. At this point the confining potential is removed and the system is further cooled down until a reasonable binding energy is attained

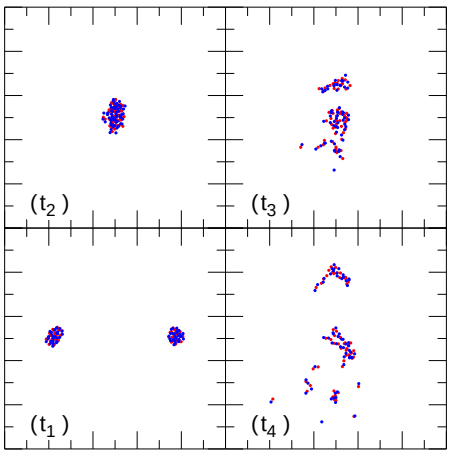

Fig. 9. Sequence of images of a central collision of Ni+Ni at an energy of 1200 MeV. The times are a 0, 300, 500 and 1200 fm/c.

For the collisions of Ni+Ni, the velocity of the projectile was boosted to the desired energy, and the projectile and target were rotated with random values of the Euler angles. Again, the evolution of the system was followed using a velocity-Verlet algorithm with an energy conservation better than 0.01%. The fragment mass distribution needed for τ was obtained from the nucleon information provided by MD using ECRA, as described in Eq. (4).

5. Conclusions

Figure 10 shows the fragment mass spectra obtained from Ni+Ni collisions at several energies. As can be seen from the shapes of these distributions, not all energies led to power-law yields, i.e. not all breakups happened at the critical point. To extract the

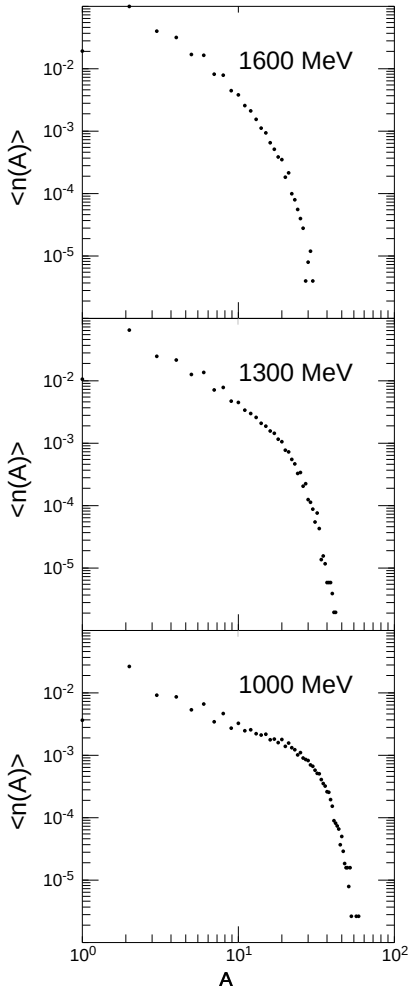

Fig. 10. Mass yields obtained from central collisions of Ni+Ni at energies of 1000, 1300 and 1600 MeV

best critical exponent, only masses in the range of $A = 2$ to 20 nucleons were used, i.e. most of their evaporation products and the target and projectile residues were eliminated. Out of the remaining data a best fit was obtained for each projectile energy, with τ values in the range of $2 \sim 3$. The best fit was obtained for a projectile energy of 1300 MeV with a multiplicity of 28, and with a resulting value of $\tau = 2.18$ with a $\chi^2 = 0.38$. Figure 11 shows the remaining data and the power-law fit obtained for this case. This value of τ agrees with the experimental value reported by the EOS Collaboration. The observed variation of τ provides enough evidence to suspect that nucleation was at work and confirms previous studies of Ni+Ni central collision, where the critical behavior was predicted to be in this projectile energy range [26].

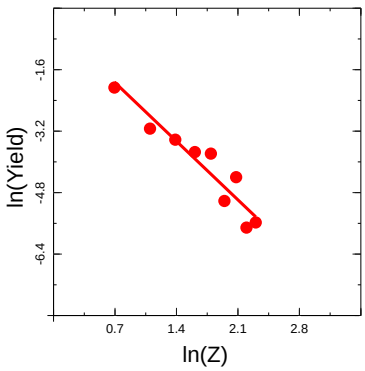

Fig. 11. Best fit of Ni+Ni central collisions at energy of 1300 MeV and a multiplicity of 28 yielding to a critical exponent of $\tau = 2.18$

Table 1 lists all the values of τ obtained for the four calculations discussed in this manuscript. The percolation results underline the fact that power law yields can be obtained from the subdivision of *small* grids of different geometries. The MD results show that nucleation appears to take place in the disassembly of small and transient compound systems. The grand conclusion is that critical phenomena appears to be possible in nuclear fragmentation.

Table 1. Summary of τ

Fragmentation Model	Value of τ
Percolation of Cubic Grid	2.32 ± 0.02
Percolation of Spherical Grid	2.20 ± 0.1
MD Simulations of 2-D Collisions	2.32 ± 0.02
MD Simulations of 3-D Collisions	2.18

Acknowledgements

Work supported by the National Science Foundation (PHY-96-00038), the Universidad de Buenos Aires (EX-070, Grant No. TW98, and CONICET Grant No. PIP 4436/96), and the Universidad Autónoma Metropolitana (Computer Laboratory grant). J.L. Acknowledges the kind hospitality of the Instituto de Física of the Universidad Nacional Autónoma de México where part of this work was carried out.

References

1. A.D. Panagiotou et al., *Phys. Rev. Lett.* **52** (1984) 496.
2. A.S. Hirsh et al., *Phys. Rev.* **C29** (1984) 508.
3. G.F. Bertsch and P. Siemens, *Nucl. Phys.* **A314** (1984) 465.
4. A.L. Goodman, J.I. Kapusta and A.Z. Mekjian, *Phys. Rev.* **C30** (1984) 851.
5. A.S. Hirsch et al., *Phys. Rev.* **C29** (1984) 508.
6. D.H.E. Gross, *Phys. Rep.* **279** (1997) 119.
7. J. Kapusta, *Phys. Rev.* **C29** (1984) 1735.
8. J. López and P. Siemens, *Nucl. Phys.* **A314** (1984) 465.
9. V. Serfling et al., *Phys. Rev. Lett.* **80** (1984) 3928.
10. J. Pochodzalla et al., *Phys. Rev. Lett.* **75** (1995) 1040.
11. M. Belkacem, V. Latora and A. Bonasera, *Phys. Rev.* **C52** (1995) 271.
12. M. Kleine Berkenbusch et al., *Phys. Rev. Lett.* **88** (2002) 022701; W. Bauer et al., *Heavy Ion Phys.* **15** (2001) 217.
13. D.H. Youngblood, C.M. Rozsa, J.M. Moss, D.R. Brown and J.D. Bronson, *Phys. Rev.* **39** (1977) 1188.
14. J.A. López and C.O. Dorso, *Lecture Notes in Phase Transformations in Nuclear Matter*, World Scientific, Singapore, 2000.
15. L.D. Landau and E.M. Lifshitz, *Statistical Physics*, 3rd Ed., Part 1, Pergamon Press Ltd., New York, 1980.
16. M.E. Fisher, *Critical Phenomena, Proceedings of the International School of Physics "Enrico Fermi" Course 51*, ed. M.S. Green, Academic, New York, 1971, p. 1.
17. C.O. Dorso and J.A. López, *Phys. Rev.* **C64** (2001) 027602.
18. T. Li et al., *Phys. Rev.* **C49** (1994) 1630.
19. L. Phair, W. Bauer and C.K. Gelbke, *Phys. Lett.* **B314** (1993) 271.
20. D. Stauffer and A. Aharony, *Introduction to Percolation Theory*, Taylor and Francis, London, 1992.
21. A. Barrañón, A. Chernomoretz, C.O. Dorso and J.A. López, *Rev. Mex. Fis.* **45(S2)** (1999) 110.
22. C.O. Dorso and J. Randrup, *Phys. Lett.* **B301** (1993) 328; C.O. Dorso and J. Aichelin, *Phys. Lett.* **B345** (1995) 197; T. Reposeur, F. Sebille, V. de la Mota and C.O. Dorso, *Z. Phys.* **A357** (1997) 79.
23. A. Strachan and C.O. Dorso, *Phys. Rev.* **C55** (1997) 99; ibid. **C58** (1998) R632; ibid. **C59** (1999) 285.
24. A. Barrañón, A. Chernomoretz, C.O. Dorso and J.A. López, *Rev. Mex. Fis.* **45(S2)** (1999) 110.
25. R.J. Lenk, T.J. Schlagel and V.R. Pandharipande, *Phys. Rev.* **C42** (1990) 372; R. Lenk and V.R. Pandharipande, *Phys. Rev.* **C34** (1986) 177; T.J. Schlagel and V.R. Pandharipande, *Phys. Rev.* **C36** (1987) 162.
26. A. Barrañón, C.O. Dorso and J.A. López, *Rev. Mex. Fis.* **47(S2)** (2001) 93.